

Negligible Effects of Baryons on the Angular Momentum Scaling Relations of Galactic Dark Matter Halos

S. MICHAEL FALL¹ AND VICENTE RODRIGUEZ-GOMEZ²¹*Department of Physics and Astronomy, Johns Hopkins University, 3400 N. Charles Street, Baltimore, MD 21218, USA*²*Instituto de Radioastronomía y Astrofísica, Universidad Nacional Autónoma de México, Apdo. Postal 72-3, 58089 Morelia, Mexico*

ABSTRACT

In cosmological simulations without baryons, the relation between the specific angular momentum j_h and mass M_h of galactic dark matter halos has the well-established form $j_h \propto M_h^{2/3}$. This is invariably adopted as the starting point in efforts to understand the analogous relation between the specific angular momentum j_* and mass M_* of the stellar parts of galaxies, which are often re-expressed relative to the corresponding halo properties through the retention fractions $f_j = j_*/j_h$ and $f_M = M_*/M_h$. An important caveat here is that the adopted $j_h \propto M_h^{2/3}$ relation could, in principle, be modified by the gravitational back-reaction of baryons on dark matter (DM). We have tested for this possibility by comparing the j_h – M_h relations in the IllustrisTNG100 and TNG50 simulations that include baryons (full-physics runs) with their counterparts that do not (DM-only runs). In all cases, we find scaling relations of the form $j_h \propto M_h^\alpha$, with $\alpha \approx 2/3$ over the ranges of mass and redshift studied here: $M_h \geq 10^{10} M_\odot$ and $0 \leq z \leq 2$. The values of α are virtually identical in the full-physics and DM-only runs at the same redshift. The only detectable effect of baryons on the j_h – M_h relation is a slightly higher normalization, by 12%–15% at $z = 0$ and by 5% at $z = 2$. This implies that existing estimates of f_j based on DM-only simulations should be adjusted downward by similar amounts. Finally, we discuss briefly some implications of this work for studies of galaxy formation.

Keywords: Galaxy formation (595) — Galaxy kinematics (602) — Galaxy dark matter halos (1880) — Hydrodynamical simulations (767) — Scaling relations (2031)

1. INTRODUCTION

Two of the most basic properties of cosmic structures are their mass M and angular momentum J or, equivalently, M and specific angular momentum $j = J/M$. The relation between j and M for a population of objects reflects the physical processes by which they form and evolve. In cold dark matter-type cosmologies, bound structures in virial equilibrium develop from small perturbations in the early universe by gravitational instability. Throughout this development, but especially in the translinear phase of growth, they acquire angular momentum from the tidal torques exerted by neighboring perturbations (Peebles 1969; Doroshkevich 1970; White 1984).

These processes are now well understood in cosmologies that include only gravitationally interacting dark matter (DM), usually thought to provide a good description of galactic halos. The results of cosmological N -body simulations are often expressed in terms of the spin parameter $\lambda \equiv j|E|^{1/2}/(GM^{3/2})$, where E is the total energy (potential plus kinetic) of a halo, and G is the gravitational con-

stant. The median spin value, derived from many DM-only (DMO) simulations, is $\hat{\lambda} \approx 0.035$, irrespective of cosmological parameters and the mass and density contrast of the halos (Bullock et al. 2001; van den Bosch et al. 2002; Avila-Reese et al. 2005; Bett et al. 2007; Macciò et al. 2007, 2008; Zjupa & Springel 2017). This implies a relation between the specific angular momentum j , mass M , and mean internal density $\langle \rho \rangle$ of halos of the form $j \propto \langle \rho \rangle^{-1/6} M^{2/3}$ (given the scalings $E \propto M^2/R$ and $\langle \rho \rangle \propto M/R^3$ with mass M and radius R). For a fixed density contrast, $\langle \rho \rangle / \rho_{\text{crit}} = \text{constant}$, this becomes $j \propto M^{2/3}$. The same simulations show that the dispersions of λ and j about their median values at each M are substantial: $\sigma(\ln \lambda) \approx \sigma(\ln j) \approx 0.5$ – 0.6 .

The optically visible stellar components of galaxies obey a remarkably similar scaling relation: $j = AM^\alpha$, with an exponent $\alpha \approx 0.6$ and an amplitude A that correlates with disk fraction and morphological type (Fall 1983; Romanowsky & Fall 2012; Fall & Romanowsky 2013; Obreschkow & Glazebrook 2014; Fall & Romanowsky 2018; Posti et al. 2018; Di Teodoro et al. 2021; Mancera Piña et al. 2021a,b; Hardwick et al. 2022; Di Teodoro et al. 2023; Pulsoni et al. 2023). This apparently simple stellar j – M relation is less straightforward to interpret than the corresponding halo relation because it must reflect the complicated combined effects of cooling, collapse, star formation, black hole growth, and

feedback in the baryonic components of galaxies. With this in mind, it is often useful to re-express the stellar j - M relation relative to the better-understood halo relation in terms of the “retention fractions” for mass, $f_M \equiv M_*/M_h$, and specific angular momentum, $f_j \equiv j_*/j_h$, the subscripts $*$ and h now specifying stellar and halo quantities explicitly. The mass retention fraction f_M is also known as the stellar-to-halo mass relation (SHMR).

In calculations of the retention fraction for specific angular momentum f_j , the reference j - M relation is invariably taken to be the one derived from DMO simulations, $j_h \propto M_h^{2/3}$. This is equivalent to assuming, at least implicitly, that the baryonic processes involved in the formation of the luminous bodies of galaxies have a negligible effect on the halo j - M relation. While plausible, this is not guaranteed to be true. Indeed, [Du et al. \(2022\)](#) have suggested that the gravitational back-reaction of baryons on the halo j - M relation is significant and necessary to explain the observed stellar j - M relation and the associated retention fraction f_j . We tested for this possibility during our recent comprehensive study of galactic angular momentum in the IllustrisTNG simulations ([Rodriguez-Gomez et al. 2022](#)) and reached a different conclusion. The purpose of this Letter is to present the results of these tests.

2. SIMULATIONS AND ANALYSIS

We examine the j - M and λ - M relations of halos in four simulations of the IllustrisTNG suite: the TNG100 and TNG50 runs, which include both baryons and DM, and their DMO counterparts, TNG100-Dark and TNG50-Dark. Our analysis is based on quantities we have computed from the positions and velocities of particles at different snapshots in the publicly accessible IllustrisTNG data files ([Nelson et al. 2019a](#)). For complete descriptions of the simulations, we refer interested readers to the original papers ([Marinacci et al. 2018](#); [Naiman et al. 2018](#); [Nelson et al. 2018](#); [Pillepich et al. 2018](#); [Springel et al. 2018](#); [Nelson et al. 2019b](#); [Pillepich et al. 2019](#)). Here, we provide only a brief summary, sufficient to interpret the results presented in Section 3.

The TNG100 and TNG50 runs include plausible subgrid prescriptions for star formation and black hole growth, as well as feedback from supernovae and active galactic nuclei (AGNs). We refer to them as “full-physics” (FP) runs. These simulations produce populations of galaxies that resemble real ones in many respects, including galactic masses and specific angular momenta ([Du et al. 2022](#); [Rodriguez-Gomez et al. 2022](#)). The main differences between the TNG100 and TNG50 runs are their volumes (cubes with comoving ~ 100 Mpc and ~ 50 Mpc sides) and numerical resolutions ($7.5 \times 10^6 M_\odot$ for DM and $1.4 \times 10^6 M_\odot$ for baryons in TNG100, and 16 times better for both in TNG50). Thus, TNG100 is preferred for studies of massive galaxy populations and TNG50 for low-mass populations. The DMO runs have the same volumes and initial conditions as the corresponding FP runs. To make precise comparisons between the simulations with and without baryons, we have matched the halos in the DMO runs individually with their counterparts

in the FP runs using the procedure described by [Rodriguez-Gomez et al. \(2017\)](#).

Halos in the simulations are identified by the friends-of-friends (FoF) algorithm ([Davis et al. 1985](#)) and gravitationally bound subhalos within them by the SUBFIND algorithm ([Springel et al. 2001](#); [Dolag et al. 2009](#)). Following standard practice, we measure positions within each halo relative to the most tightly bound particle and velocities relative to the center-of-mass motion¹ ([Genel et al. 2015](#); [Zjupa & Springel 2017](#)). We compute all halo quantities, denoted by the subscript h , by including both DM and baryons within $R_h \equiv R_{200,\text{crit}}$, the radius enclosing the mean density $\langle \rho \rangle = 200\rho_{\text{crit}}$ (aka the “virial radius”); hence, $M_h \equiv M_{200,\text{crit}}$, $J_h \equiv J_{200,\text{crit}}$, and $j_h \equiv J_h/M_h$.² As an approximation to the spin parameter λ , we compute the analogous quantity $\lambda' \equiv j_h/(\sqrt{2}R_h V_h)$, where $V_h = (GM_h/R_h)^{1/2}$ is the circular velocity at the virial radius ([Bullock et al. 2001](#)). For a singular isothermal halo, λ' is exactly the same as λ (in the limit $\lambda \ll 1$).

Galaxies in the simulations consist of all the star particles and gas elements within the subhalos identified by SUBFIND. For each FoF halo, this algorithm assigns a smooth central or “background” subhalo by removing all its satellite subhalos while checking that it remains gravitationally bound ([Springel et al. 2001](#), Figure 3). Thus, central galaxies—which we consider exclusively throughout this work—consist of all the baryonic material associated with these central subhalos. We specify galactic morphology in terms of the parameter κ_{rot} , defined as the fraction of the stellar kinetic energy invested in rotation ([Sales et al. 2010](#); [Rodriguez-Gomez et al. 2017](#)). In particular, we classify galaxies with $\kappa_{\text{rot}} < 0.5$ as spheroid dominated and those with $\kappa_{\text{rot}} \geq 0.5$ as disk dominated. We compute the stellar properties of galaxies, such as M_* and κ_{rot} , by summing over all the stars bound to their subhalos.

3. RESULTS

The main results of this Letter—comparisons between the halo j - M and λ' - M relations in the FP and DMO IllustrisTNG simulations—are displayed in Figures 1–3 and Table 1. For these comparisons, we have performed linear regressions of the form

$$\log j_h = \alpha \log \left(\frac{M_h}{10^{12} M_\odot} \right) + \log j_{h,12} \quad (1)$$

$$\log \lambda' = \beta \log \left(\frac{M_h}{10^{12} M_\odot} \right) + \log \lambda'_{12} \quad (2)$$

to determine the best-fit slopes α and β and normalizations $\log j_{h,12}$ and $\log \lambda'_{12}$. We then compute the standard (i.e.,

¹ The specific angular momentum computed in this reference frame is exactly the same as that in a frame defined by both the center-of-mass position and velocity, as one can show by simple algebra.

² Note that, by definition, halo quantities such as M_h and j_h include all material within R_h in both the central and satellite subhalos as well as any unbound particles (aka “fuzz”).

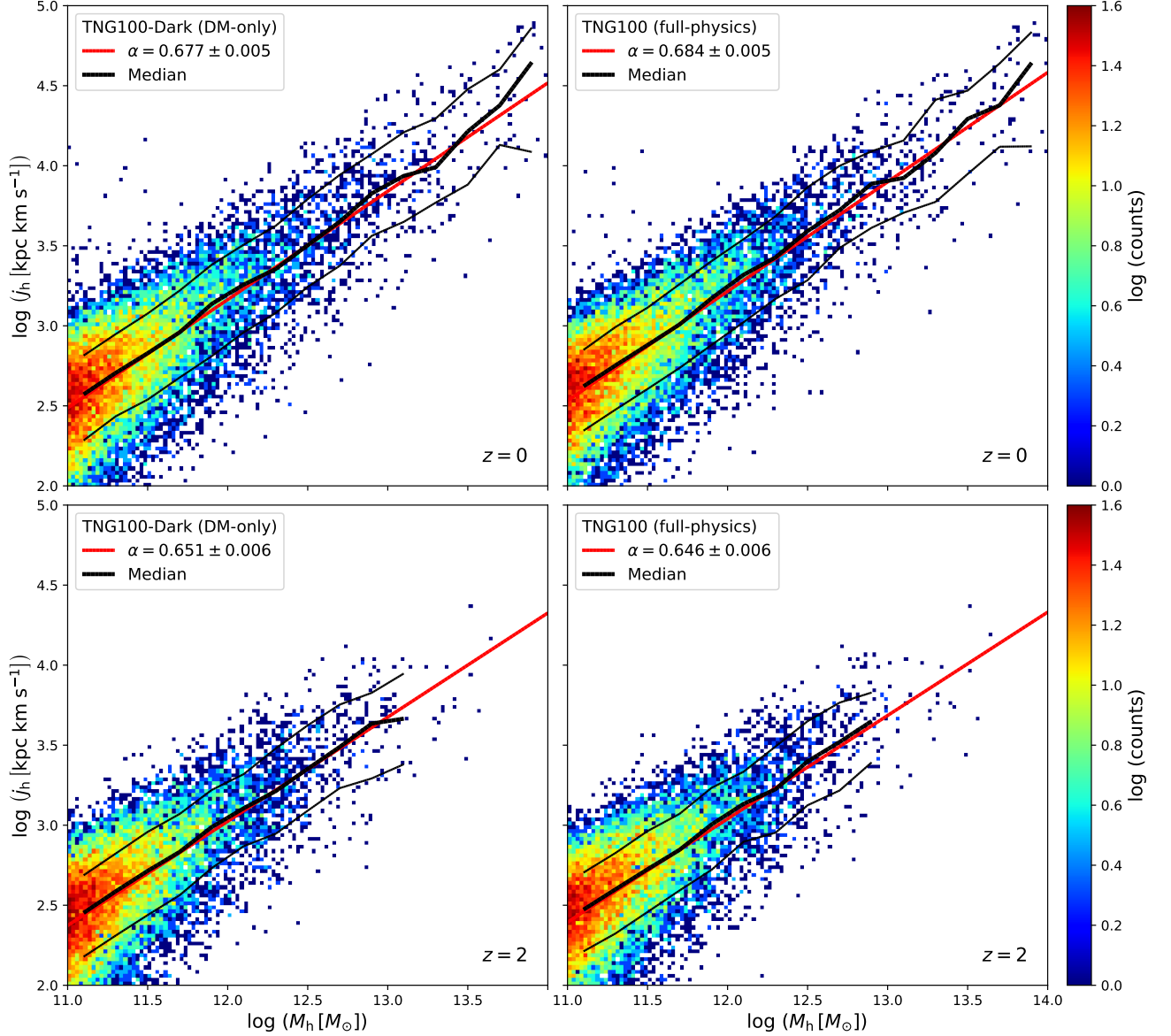


Figure 1. Specific angular momentum j_h plotted against mass M_h for halos in the TNG100 DMO and FP runs (left and right panels, respectively) at redshifts $z = 0$ and $z = 2$ (upper and lower panels, respectively). The color scale indicates the number of halos in each 2D bin. The red lines represent the best-fit linear relations, while the black lines represent the running median relations and 16th–84th percentile ranges. Note the close similarity of the halo j – M relations in the DMO and FP runs and the slightly flatter slopes at $z = 2$ than at $z = 0$.

1σ) errors of these quantities by bootstrap resampling. The figures and table present results for two redshifts, $z = 0$ and $z = 2$, and several different selection criteria specified by lower limits on halo mass M_h , stellar mass M_* , and morphology parameter κ_{rot} .

We have adopted these redshifts and selection criteria with the following thoughts in mind. Because the masses of individual halos grow with time, so also does the upper extent of their j – M relation (compare the upper and lower panels of Figure 1). As a result, the available range of masses shrinks with increasing redshift, and above $z \sim 2$, it becomes too narrow to determine the slopes α and β reliably. The restrictions on halo masses, $M_h \geq 10^{11} M_\odot$ for TNG100 and

$M_h \geq 10^{10} M_\odot$ for TNG50, were chosen to compensate approximately for the different resolutions and volumes of these simulations. These limits are also intended to exclude the low-mass galaxies that might suffer from the spurious heating of stellar motions by DM particles and the resulting transfer of angular momentum to their halos (Ludlow et al. 2021; Wilkinson et al. 2023). We have also checked what happens to the fitted slopes α and β when we impose the same selection criteria as Du et al. (2022) on the stellar properties of galaxies, namely $M_* \geq 10^9 M_\odot$ and $\kappa_{\text{rot}} \geq 0.5$.

We first compare the halo j – M and λ' – M relations in the FP and DMO runs in samples defined by halo properties alone, specifically $M_h \geq 10^{11} M_\odot$ for TNG100 and

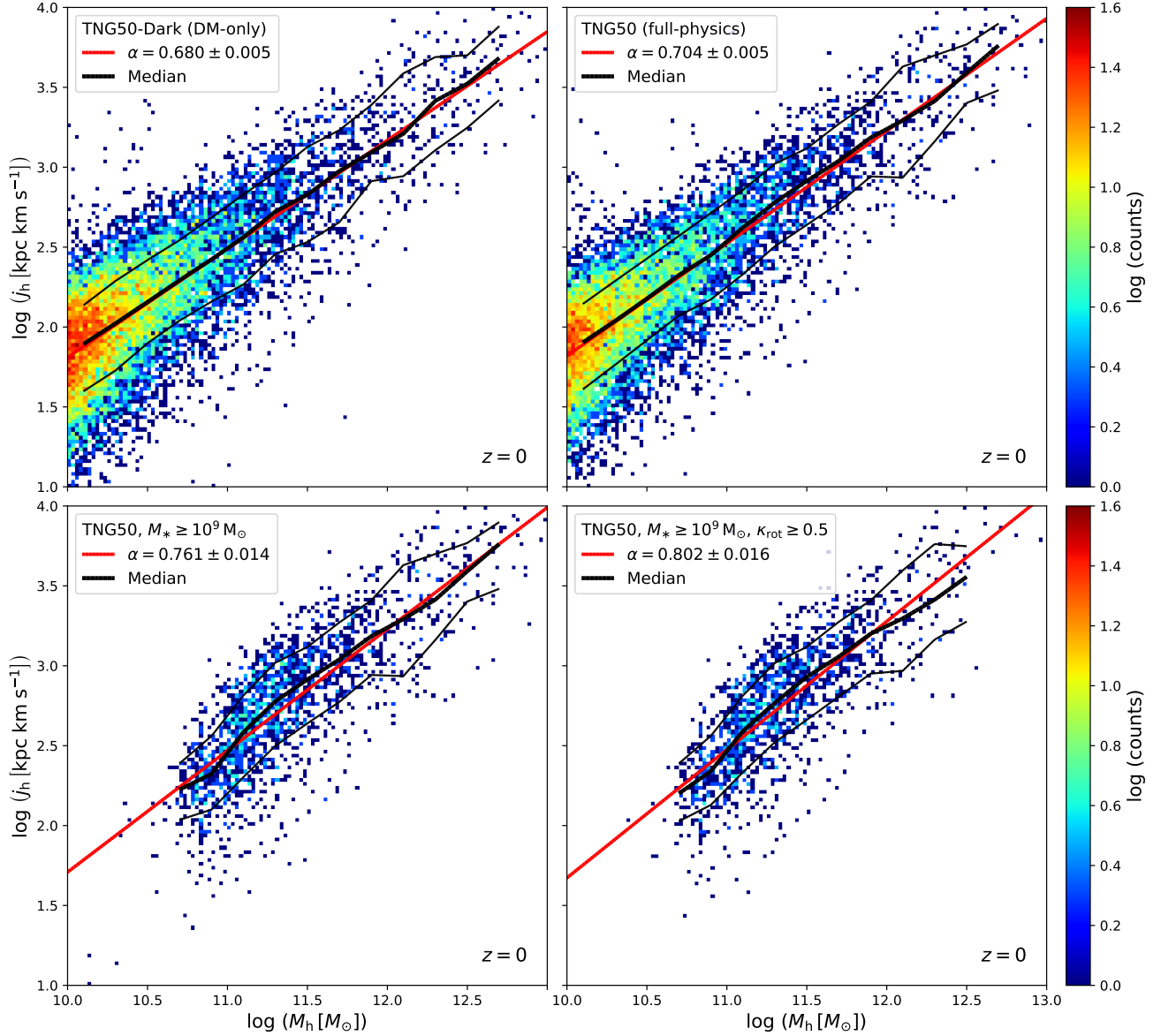


Figure 2. Specific angular momentum j_h plotted against mass M_h for halos in the TNG50 DMO and FP runs at $z = 0$ (upper left and upper right panels, respectively) and the FP run at $z = 0$ with selection criteria based on the stellar masses and morphologies of galaxies: $M_* \geq 10^9 M_\odot$ (lower left panel) and $M_* \geq 10^9 M_\odot$ and $\kappa_{\text{rot}} \geq 0.5$ (lower right panel). The last of these replicates the selection criteria adopted by [Du et al. \(2022\)](#). The color scale indicates the number of halos in each 2D bin. The red lines represent the best-fit linear relations, while the black lines represent the running median relations and 16th–84th percentile ranges. Note the close similarity of the halo j – M relations in the DMO and FP runs and the steeper fitted slopes in the samples selected by stellar properties.

$M_h \geq 10^{10} M_\odot$ for TNG50. The upper and lower panels of Figure 1 show the halo j – M relation in the TNG100 FP and DMO runs at $z = 0$ and $z = 2$, while the upper panels of Figure 2 show the same results for TNG50 at $z = 0$. Table 1 lists the slopes α and β of the halo j – M and λ' – M relations in all the simulations at $z = 0$ and $z = 2$. In all cases, these are close to the expected values $\alpha = 2/3$ and $\beta = 0$. Furthermore, the slopes in the FP runs are nearly the same as those in the corresponding DMO runs, with $\Delta\alpha \approx \Delta\beta < 0.01$ for TNG100 and $\Delta\alpha \approx \Delta\beta < 0.03$ for TNG50. However, for

both TNG100 and TNG50, the normalizations of the halo j – M and λ' – M relations are slightly higher in the FP runs than in the DMO runs, by $\Delta \log j_{h,12} \approx \Delta \log \lambda'_{12} \approx 0.05$ – 0.06 (12%–15%) at $z = 0$ and ≈ 0.02 (5%) at $z = 2$. We also find that these relations are slightly flatter at $z = 2$ than at $z = 0$, by $\Delta\alpha \approx \Delta\beta \approx 0.02$ – 0.05 for both TNG100 and TNG50.

We can elucidate these results by comparing the masses M_h , specific angular momenta j_h , and spin parameters λ' of halos in the FP runs with those of their individually matched counterparts in the DMO runs. These com-

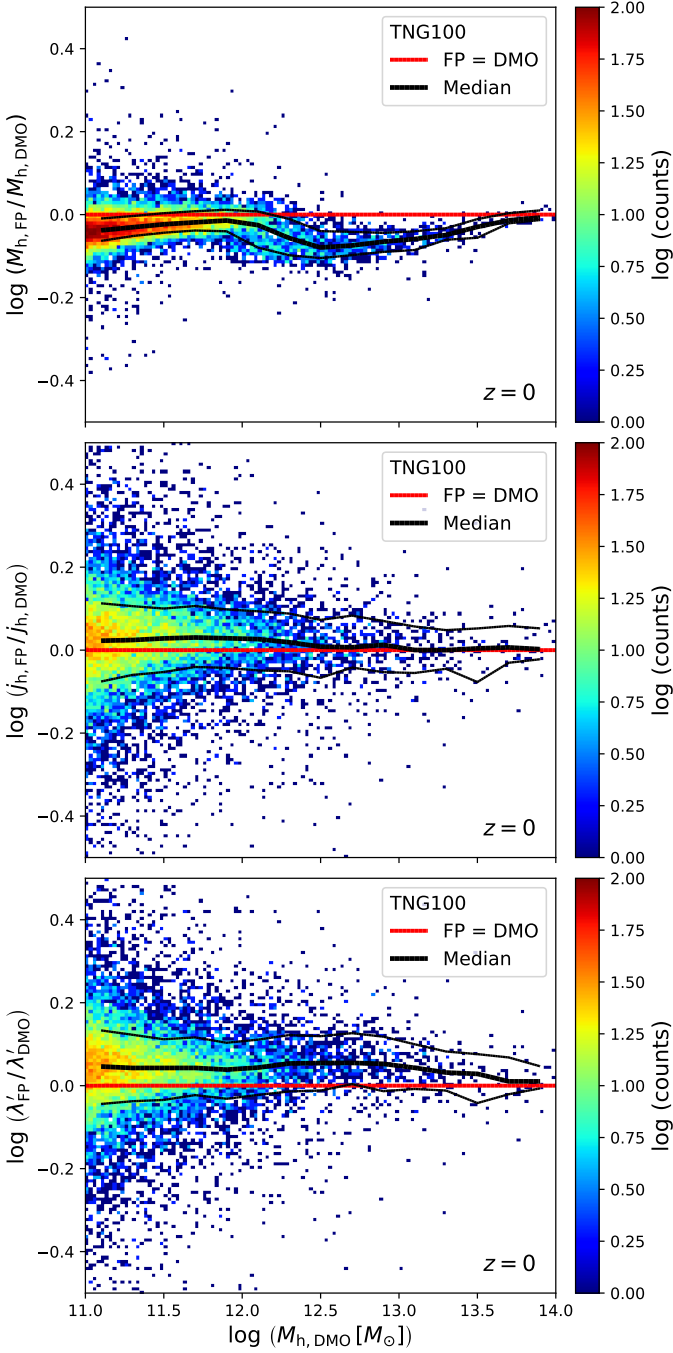


Figure 3. Ratios of mass M_h (top panel), specific angular momentum j_h (middle panel), and spin parameter λ' (bottom panel) for halos in the FP run to the same quantities for the individually matched halos in the DMO run plotted against mass $M_{h, \text{DMO}}$ for TNG100 at $z = 0$. The color scale indicates the number of halos in each 2D bin. The red horizontal lines indicate equality, while the black lines represent the running median relations and 16th–84th percentile ranges. This diagram shows directly the effects of baryons on the halo properties M_h , j_h , and λ' . Note the relatively small and nearly constant median offset of λ'_{FP} from λ'_{DMO} , indicating that the halo relation $j_h \propto M_h^\alpha$ with $\alpha \approx 2/3$ is preserved by baryonic processes.

parisons are shown in Figure 3, where we plot the ratios $M_{h, \text{FP}}/M_{h, \text{DMO}}$, $j_{h, \text{FP}}/j_{h, \text{DMO}}$, and $\lambda'_{\text{FP}}/\lambda'_{\text{DMO}}$ against $M_{h, \text{DMO}}$ for the TNG100 simulation at $z = 0$. Evidently, baryons have a rather complex effect on the median offset between $M_{h, \text{FP}}$ and $M_{h, \text{DMO}}$, likely caused by the varying strengths of supernova and AGN feedback, but they introduce relatively little scatter about this trend (top panel). In contrast, the median offsets between $j_{h, \text{FP}}$ and $j_{h, \text{DMO}}$ and between λ'_{FP} and λ'_{DMO} are small and nearly constant, while the scatter about these trends is large (middle and bottom panels). Since the spin parameter can be re-expressed as $\lambda' \propto \langle \rho \rangle^{1/6} j_h / M_h^{2/3} \propto j_h / M_h^{2/3}$ (at fixed $\langle \rho \rangle / \rho_{\text{crit}}$), the nearly constant median offset of λ' with M_h ensures that the relation $j_h \propto M_h^\alpha$ with $\alpha \approx 2/3$ is preserved, but with a 12%–15% higher amplitude, consistent with the results listed in Table 1.

Why does the inclusion of baryons in the simulations make so little difference to the halo j – M relation? There are three contributing factors, corresponding to the quantities M , j , and E that appear in the formula for λ (and hence λ'). First, the fraction of mass in baryons is small compared with that in DM (16% vs 84%). Second, while the baryons within individual halos can gain or lose large amounts of specific angular momentum, there is little net transfer within the population of halos as a whole. Third, the ratios of the specific binding energies of circumgalactic baryons and DM particles within the same halos, as measured by their kinetic temperatures, are of order unity and increase only gradually with mass. These factors help to explain the results shown in Figure 3, particularly the near constancy of λ' with M_h and thus $j_h \propto M_h^{2/3}$.

The preceding results indicate that baryons have negligible *physical* effects on the slope α of the halo j – M relation in the IllustrisTNG simulations. This does not mean, however, that this slope will always be the same for samples of galaxies selected by different baryonic properties, such as stellar mass M_* and morphology parameter κ_{rot} . In these cases, there can be non-negligible *apparent* effects on α . This is illustrated for TNG50 at $z = 0$ in the lower panels of Figure 2—on the left for the restriction $M_* \geq 10^9 M_\odot$ alone and on the right when combined with the restriction $\kappa_{\text{rot}} \geq 0.5$. The latter mimics a luminosity-limited sample of disk-dominated galaxies. In this case, we find $\alpha \approx 0.8$, similar to the slope Du et al. (2022) found. The reason for this apparent increase in α can be traced to the fact that a vertical cut in the j_h – M_* plane maps into a diagonal cut in the j_h – M_h plane, as shown in the lower panels of Figure 2 here and in Figure 5 of Du et al. (2022). Consequently, the fitted slope of the halo j – M relation for this particular sample is slightly steeper than that for the underlying population.

4. DISCUSSION

Our main conclusion is that the halo j – M and λ' – M relations in the IllustrisTNG simulations are very close to the expected forms, $j_h \propto M_h^{2/3}$ and $\lambda' \propto M_h^0$, at least over the ranges of mass and redshift examined here: $M_h \geq 10^{10} M_\odot$

Table 1. Regression Fits to Equations (1) and (2) for Different Simulations, Redshifts, and Selection Criteria.

Simulation (1)	Redshift (2)	Selection criteria (3)	α (4)	$\log j_{h,12}$ (5)	β (6)	$\log \lambda'_{12}$ (7)
TNG100 $z = 0$						
DM-only		$M_h \geq 10^{11} M_\odot$	0.677 ± 0.005	3.164 ± 0.003	0.010 ± 0.005	-1.464 ± 0.003
Full-physics		$M_h \geq 10^{11} M_\odot$	0.684 ± 0.005	3.215 ± 0.003	0.017 ± 0.005	-1.412 ± 0.003
Full-physics		$M_* \geq 10^9 M_\odot$	0.746 ± 0.005	3.212 ± 0.003	0.080 ± 0.005	-1.416 ± 0.003
Full-physics		$M_* \geq 10^9 M_\odot, \kappa_{\text{rot}} \geq 0.5$	0.781 ± 0.007	3.244 ± 0.004	0.114 ± 0.007	-1.384 ± 0.004
TNG50						
DM-only		$M_h \geq 10^{10} M_\odot$	0.680 ± 0.005	3.169 ± 0.008	0.013 ± 0.005	-1.459 ± 0.008
Full-physics		$M_h \geq 10^{10} M_\odot$	0.704 ± 0.005	3.227 ± 0.008	0.038 ± 0.005	-1.399 ± 0.008
Full-physics		$M_* \geq 10^9 M_\odot$	0.761 ± 0.014	3.230 ± 0.010	0.094 ± 0.014	-1.397 ± 0.010
Full-physics		$M_* \geq 10^9 M_\odot, \kappa_{\text{rot}} \geq 0.5$	0.802 ± 0.016	3.278 ± 0.013	0.136 ± 0.016	-1.349 ± 0.013
TNG100 $z = 2$						
DM-only		$M_h \geq 10^{11} M_\odot$	0.651 ± 0.006	3.024 ± 0.004	-0.014 ± 0.006	-1.431 ± 0.004
Full-physics		$M_h \geq 10^{11} M_\odot$	0.646 ± 0.006	3.040 ± 0.004	-0.018 ± 0.006	-1.409 ± 0.004
Full-physics		$M_* \geq 10^9 M_\odot$	0.746 ± 0.007	3.044 ± 0.004	0.080 ± 0.007	-1.405 ± 0.004
Full-physics		$M_* \geq 10^9 M_\odot, \kappa_{\text{rot}} \geq 0.5$	0.730 ± 0.012	3.017 ± 0.006	0.064 ± 0.012	-1.431 ± 0.006
TNG50						
DM-only		$M_h \geq 10^{10} M_\odot$	0.659 ± 0.005	3.026 ± 0.008	-0.006 ± 0.005	-1.427 ± 0.008
Full-physics		$M_h \geq 10^{10} M_\odot$	0.650 ± 0.005	3.042 ± 0.008	-0.013 ± 0.005	-1.403 ± 0.008
Full-physics		$M_* \geq 10^9 M_\odot$	0.722 ± 0.020	3.031 ± 0.013	0.056 ± 0.020	-1.415 ± 0.013
Full-physics		$M_* \geq 10^9 M_\odot, \kappa_{\text{rot}} \geq 0.5$	0.683 ± 0.030	2.983 ± 0.017	0.016 ± 0.030	-1.463 ± 0.017

NOTE—The quoted 1σ errors were derived by bootstrap resampling.

and $0 \leq z \leq 2$. This is true for both TNG100 and TNG50 and for both FP and DMO runs. We find some deviations from the canonical slopes $\alpha = 2/3$ and $\beta = 0$ that are statistically significant given the exceedingly small formal errors listed in Table 1. However, these small deviations are comparable to the differences in α and β between the TNG100 and TNG50 simulations and are likely negligible for all practical purposes. In particular, the assumed halo j – M relation with $\alpha = 2/3$ is sufficiently accurate to estimate the retention fractions of specific angular momentum, $f_j = j_*/j_h$, from the observed stellar j – M relations for low-redshift galaxies. Beyond $z \approx 2$, the reference value of α may be slightly lower than $2/3$.

The halo j – M relation—in the form confirmed here—when combined with the observed stellar j – M relation, provides an important link between the retention fractions f_M and f_j , and with it some valuable insights into galaxy formation, as we now summarize briefly. For the power-law models, $j_* = A_* M_*^{\alpha_*}$ and $j_h = A_h M_h^{\alpha_h}$, we have

$$f_j/f_M^{\alpha_h} = (A_*/A_h) M_*^{\alpha_* - \alpha_h} \sim \text{constant}. \quad (3)$$

Given the small difference between the exponents of the stellar and halo j – M relations ($\alpha_* \approx 0.6$ vs $\alpha_h = 2/3$), Equation (3) indicates that f_j and f_M will have similar shapes al-

though the former will be subdued relative to the latter. This is interesting because recent dynamical studies have revealed that the high-mass shape of the SHMR depends strongly on galactic morphology (Posti et al. 2019a,b; Posti & Fall 2021; Di Teodoro et al. 2023). For disk-dominated galaxies, f_M rises monotonically with mass, with no prominent features, while for spheroid-dominated galaxies, f_M has the more familiar, inverted-U shape, with a peak near the mass of the Milky Way. Another simple consequence of Equation (3) is that the value of f_j for each type of galaxy scales directly with the stellar amplitude A_* and inversely with the halo amplitude A_h .

Empirical determinations of the stellar j – M relation require both photometric and kinematic data, ideally covering each galaxy in a large sample in two dimensions to large radii. For spiral galaxies, the stellar j – M relation is quite secure; all determinations, including the original one 40 yr ago, are in remarkably close agreement. This is a consequence of the known inclination of each galactic disk and the fact that the angular momentum of disks with exponential surface-density profiles and flat rotation curves converges rapidly beyond about two effective radii. Recent studies of the stellar j – M relation of low-redshift spiral galaxies all find very similar angular momentum retention fractions, $f_j \approx 0.8$, based

on A_h values from DMO simulations, with little or no dependence on mass (Fall & Romanowsky 2013, 2018; Posti et al. 2018, 2019b; Di Teodoro et al. 2021, 2023). Adjusting this for the higher A_h values in simulations with baryons gives $f_j \approx 0.7$. A corollary of this result is that, on average, the exponential scale radii R_d of galactic disks are related to the virial radii R_h of their halos by $R_d/R_h \approx f_j \hat{\lambda}/\sqrt{2} \sim 0.02$ (Fall & Efstathiou 1980; Fall 1983; Mo et al. 1998; note the changes in notation, $\alpha \rightarrow 1/R_d$ and $r_t \rightarrow R_h$, between the early and later papers and the fact that the product $f_j \hat{\lambda}$ is independent of the A_h adjustment).

Determinations of the stellar j - M relations of lenticular and elliptical galaxies are much harder because the inclinations of the galaxies are uncertain, the shapes of the rotation curves vary, the angular momenta converge slowly, and kinematic data are sparse at large radii. The resulting estimates of the angular momentum retention fractions of spheroid-dominated galaxies are $f_j \sim 0.1$, with an uncertain mass de-

pendence (Romanowsky & Fall 2012; Fall & Romanowsky 2013, 2018; Pulsoni et al. 2023). The observed order-of-magnitude difference between the values of f_j for disk- and spheroid-dominated galaxies are also found in simulations of galaxy formation (Genel et al. 2015; Pedrosa & Tissera 2015; Teklu et al. 2015; Zavala et al. 2016; Sokołowska et al. 2017; El-Badry et al. 2018; Rodriguez-Gomez et al. 2022). One of the key challenges in theoretical studies of galaxy formation is to provide a compelling physical explanation for this large difference in angular momentum retention. In effect, this would also serve as an explanation for the main morphological characteristics of galaxies embodied in the Hubble classification scheme.

We thank Min Du for interesting correspondence on this topic and Shy Genel for collaboration on the earlier project from which this one developed.

REFERENCES

- Avila-Reese, V., Colin, P., Gottlober, S., Firmani, C., & Maulbetsch, C. 2005, *ApJ*, 634, 51, doi: [10.1086/491726](https://doi.org/10.1086/491726)
- Bett, P., Eke, V., Frenk, C. S., et al. 2007, *MNRAS*, 376, 215, doi: [10.1111/j.1365-2966.2007.11432.x](https://doi.org/10.1111/j.1365-2966.2007.11432.x)
- Bullock, J. S., Dekel, A., Kolatt, T. S., et al. 2001, *ApJ*, 555, 240, doi: [10.1086/321477](https://doi.org/10.1086/321477)
- Davis, M., Efstathiou, G., Frenk, C. S., & White, S. D. M. 1985, *ApJ*, 292, 371, doi: [10.1086/163168](https://doi.org/10.1086/163168)
- Di Teodoro, E. M., Posti, L., Ogle, P. M., Fall, S. M., & Jarrett, T. 2021, *MNRAS*, 507, 5820, doi: [10.1093/mnras/stab2549](https://doi.org/10.1093/mnras/stab2549)
- Di Teodoro, E. M., Posti, L., Fall, S. M., et al. 2023, *MNRAS*, 518, 6340, doi: [10.1093/mnras/stac3424](https://doi.org/10.1093/mnras/stac3424)
- Dolag, K., Borgani, S., Murante, G., & Springel, V. 2009, *MNRAS*, 399, 497, doi: [10.1111/j.1365-2966.2009.15034.x](https://doi.org/10.1111/j.1365-2966.2009.15034.x)
- Doroshkevich, A. G. 1970, *Astrofizika*, 6, 581, doi: [10.1007/BF01001625](https://doi.org/10.1007/BF01001625)
- Du, M., Ho, L. C., Yu, H.-R., & Debattista, V. P. 2022, *ApJ*, 937, L18, doi: [10.3847/2041-8213/ac911e](https://doi.org/10.3847/2041-8213/ac911e)
- El-Badry, K., Quataert, E., Wetzel, A., et al. 2018, *MNRAS*, 473, 1930, doi: [10.1093/mnras/stx2482](https://doi.org/10.1093/mnras/stx2482)
- Fall, S. M. 1983, in *IAU Symp. 100, Internal Kinematics and Dynamics of Galaxies*, ed. E. Athanassoula (Cambridge: Cambridge Univ. Press), 391
- Fall, S. M., & Efstathiou, G. 1980, *MNRAS*, 193, 189, doi: [10.1093/mnras/193.2.189](https://doi.org/10.1093/mnras/193.2.189)
- Fall, S. M., & Romanowsky, A. J. 2013, *ApJ*, 769, L26, doi: [10.1088/2041-8205/769/2/L26](https://doi.org/10.1088/2041-8205/769/2/L26)
- . 2018, *ApJ*, 868, 133, doi: [10.3847/1538-4357/aab27](https://doi.org/10.3847/1538-4357/aab27)
- Genel, S., Fall, S. M., Hernquist, L., et al. 2015, *ApJ*, 804, L40, doi: [10.1088/2041-8205/804/2/L40](https://doi.org/10.1088/2041-8205/804/2/L40)
- Hardwick, J. A., Cortese, L., Obreschkow, D., Catinella, B., & Cook, R. H. W. 2022, *MNRAS*, 509, 3751, doi: [10.1093/mnras/stab3261](https://doi.org/10.1093/mnras/stab3261)
- Ludlow, A. D., Fall, S. M., Schaye, J., & Obreschkow, D. 2021, *MNRAS*, 508, 5114, doi: [10.1093/mnras/stab2770](https://doi.org/10.1093/mnras/stab2770)
- Macciò, A. V., Dutton, A. A., & van den Bosch, F. C. 2008, *MNRAS*, 391, 1940, doi: [10.1111/j.1365-2966.2008.14029.x](https://doi.org/10.1111/j.1365-2966.2008.14029.x)
- Macciò, A. V., Dutton, A. A., Van Den Bosch, F. C., et al. 2007, *MNRAS*, 378, 55, doi: [10.1111/j.1365-2966.2007.11720.x](https://doi.org/10.1111/j.1365-2966.2007.11720.x)
- Mancera Piña, P. E., Posti, L., Fraternali, F., Adams, E. A. K., & Oosterloo, T. 2021a, *A&A*, 647, A76, doi: [10.1051/0004-6361/202039340](https://doi.org/10.1051/0004-6361/202039340)
- Mancera Piña, P. E., Posti, L., Pezzulli, G., et al. 2021b, *A&A*, 651, L15, doi: [10.1051/0004-6361/202141574](https://doi.org/10.1051/0004-6361/202141574)
- Marinacci, F., Vogelsberger, M., Pakmor, R., et al. 2018, *MNRAS*, 5139, 5113, doi: [10.1093/mnras/sty2206](https://doi.org/10.1093/mnras/sty2206)
- Mo, H. J., Mao, S., & White, S. D. M. 1998, *MNRAS*, 295, 319, doi: [10.1046/j.1365-8711.1998.01227.x](https://doi.org/10.1046/j.1365-8711.1998.01227.x)
- Naiman, J. P., Pillepich, A., Springel, V., et al. 2018, *MNRAS*, 477, 1206, doi: [10.1093/mnras/sty618](https://doi.org/10.1093/mnras/sty618)
- Nelson, D., Pillepich, A., Springel, V., et al. 2018, *MNRAS*, 475, 624, doi: [10.1093/mnras/stx3040](https://doi.org/10.1093/mnras/stx3040)
- Nelson, D., Springel, V., Pillepich, A., et al. 2019a, *Comput. Astrophys. Cosmol.*, 6, 2, doi: [10.1186/s40668-019-0028-x](https://doi.org/10.1186/s40668-019-0028-x)
- Nelson, D., Pillepich, A., Springel, V., et al. 2019b, *MNRAS*, 490, 3234, doi: [10.1093/mnras/stz2306](https://doi.org/10.1093/mnras/stz2306)
- Obreschkow, D., & Glazebrook, K. 2014, *ApJ*, 784, 26, doi: [10.1088/0004-637X/784/1/26](https://doi.org/10.1088/0004-637X/784/1/26)
- Pedrosa, S. E., & Tissera, P. B. 2015, *A&A*, 584, A43, doi: [10.1051/0004-6361/201526440](https://doi.org/10.1051/0004-6361/201526440)
- Peebles, P. J. E. 1969, *ApJ*, 155, 393, doi: [10.1086/149876](https://doi.org/10.1086/149876)

- Pillepich, A., Nelson, D., Hernquist, L., et al. 2018, MNRAS, 475, 648, doi: [10.1093/mnras/stx3112](https://doi.org/10.1093/mnras/stx3112)
- Pillepich, A., Nelson, D., Springel, V., et al. 2019, MNRAS, 490, 3196, doi: [10.1093/mnras/stz2338](https://doi.org/10.1093/mnras/stz2338)
- Posti, L., & Fall, S. M. 2021, A&A, 649, A119, doi: [10.1051/0004-6361/202040256](https://doi.org/10.1051/0004-6361/202040256)
- Posti, L., Fraternali, F., Di Teodoro, E. M., & Pezzulli, G. 2018, A&A, 612, L6, doi: [10.1051/0004-6361/201833091](https://doi.org/10.1051/0004-6361/201833091)
- Posti, L., Fraternali, F., & Marasco, A. 2019a, A&A, 626, A56, doi: [10.1051/0004-6361/201935553](https://doi.org/10.1051/0004-6361/201935553)
- Posti, L., Marasco, A., Fraternali, F., & Famaey, B. 2019b, A&A, 629, A59, doi: [10.1051/0004-6361/201935982](https://doi.org/10.1051/0004-6361/201935982)
- Pulsoni, C., Gerhard, O., Fall, S. M., et al. 2023, A&A, in press (arXiv:2303.06132). <http://arxiv.org/abs/2303.06132>
- Rodriguez-Gomez, V., Sales, L. V., Genel, S., et al. 2017, MNRAS, 467, 3083, doi: [10.1093/mnras/stx305](https://doi.org/10.1093/mnras/stx305)
- Rodriguez-Gomez, V., Genel, S., Fall, S. M., et al. 2022, MNRAS, 512, 5978, doi: [10.1093/mnras/stac806](https://doi.org/10.1093/mnras/stac806)
- Romanowsky, A. J., & Fall, S. M. 2012, ApJS, 203, 17, doi: [10.1088/0067-0049/203/2/17](https://doi.org/10.1088/0067-0049/203/2/17)
- Sales, L. V., Navarro, J. F., Schaye, J., et al. 2010, MNRAS, 409, 1541, doi: [10.1111/j.1365-2966.2010.17391.x](https://doi.org/10.1111/j.1365-2966.2010.17391.x)
- Sokołowska, A., Capelo, P. R., Fall, S. M., et al. 2017, ApJ, 835, 289, doi: [10.3847/1538-4357/835/2/289](https://doi.org/10.3847/1538-4357/835/2/289)
- Springel, V., White, S. D. M., Tormen, G., & Kauffmann, G. 2001, MNRAS, 328, 726, doi: [10.1046/j.1365-8711.2001.04912.x](https://doi.org/10.1046/j.1365-8711.2001.04912.x)
- Springel, V., Pakmor, R., Pillepich, A., et al. 2018, MNRAS, 475, 676, doi: [10.1093/mnras/stx3304](https://doi.org/10.1093/mnras/stx3304)
- Teklu, A. F., Remus, R.-S., Dolag, K., et al. 2015, ApJ, 812, 29, doi: [10.1088/0004-637X/812/1/29](https://doi.org/10.1088/0004-637X/812/1/29)
- van den Bosch, F. C., Abel, T., Croft, R. A. C., Hernquist, L., & White, S. D. M. 2002, ApJ, 576, 21, doi: [10.1086/341619](https://doi.org/10.1086/341619)
- White, S. D. M. 1984, ApJ, 286, 38, doi: [10.1086/162573](https://doi.org/10.1086/162573)
- Wilkinson, M. J., Ludlow, A. D., Lagos, C. d. P., et al. 2023, MNRAS, 519, 5942, doi: [10.1093/mnras/stad055](https://doi.org/10.1093/mnras/stad055)
- Zavala, J., Frenk, C. S., Bower, R., et al. 2016, MNRAS, 460, 4466, doi: [10.1093/mnras/stw1286](https://doi.org/10.1093/mnras/stw1286)
- Zjupa, J., & Springel, V. 2017, MNRAS, 466, 1625, doi: [10.1093/mnras/stw2945](https://doi.org/10.1093/mnras/stw2945)